A direct method to solve quasistatic micromagnetic problems

Insinga, Andrea Roberto; Blaabjerg Poulsen, Emil; Nielsen, Kaspar Kirstein; Bjørk, Rasmus

Published in:
Journal of Magnetism and Magnetic Materials

Link to article, DOI:
10.1016/j.jmmm.2020.166900

Publication date:
2020

Document Version
Peer reviewed version

A direct method to solve quasistatic micromagnetic problems

A. R. Insinga, E. Blaabjerg Poulsen, K. K. Nielsen and R. Bjørk

Abstract

Micromagnetic simulations are employed for predicting the behavior of magnetic materials from their microscopic properties. In this paper we focus on hysteresis loops, which are computed by assuming quasistatic conditions: i.e. the magnetization distribution remains at equilibrium while the applied magnetic field is slowly varied.

The dynamic behavior of micromagnetic systems is governed by the Landau-Lifshitz equation. In order to apply the dynamic equation to a quasistatic problem, it is necessary to artificially decouple the relaxation dynamics from the time-scale of the variation of the applied field. This decoupling is normally done in an iterative fashion: the field is considered fixed until the equilibrium point is reached, and subsequently updated. However, this approach is indirect and also has the potential issue that a system might switch to a different equilibrium configuration before the previous equilibrium becomes unstable, which is a behavior not possible in the quasistatic regime.

Instead, here we derive the differential equation, which directly describes the evolution of the equilibrium states of the Landau-Lifshitz equation as a function of the external field, or any other externally varied parameter. This approach is a more rigorous description of quasistatic processes and inherently enforces the system to follow a given equilibrium configuration until this disappears or becomes unstable. We demonstrate this approach with simple examples and show it to be as or more stable than the previously used approaches.

1 Introduction

1.1 Background and motivation

The subject of micromagnetism is the behavior of magnetic systems at the microscopic scale. At this length scale it is not necessary to employ a quantum-mechanical formalism. Instead, the system is described by the formalism of continuum mechanics: the physical mechanisms arising from quantum effects are included as phenomenological interaction terms.

The starting point in micromagnetism is the definition of the micromagnetic free energy, which takes into account the classical macroscopic magnetic interaction, as well as the exchange interaction, and the anisotropy due to the crystalline structure of the magnetic materials. A magnetization distribution is an equilibrium configuration if it is a local minimum of the free energy. The goal of micromagnetism is either to compute the equilibrium magnetization distributions, or to simulate the time-evolution of dynamical processes. These two problems are governed by Brown's equation and the Landau-Lifshitz equation, respectively. Except for simple cases, the equations can only be treated through numerical simulations.

Micromagnetic simulations are employed in several scientific fields, such as the study of permanent magnets[1, 5], magnetic storage and processing devices[11], and spintronic systems[6]. Depending on the area of application, the purpose of these simulations is different. In the present work we focus on permanent magnet systems, and in particular on the computation of

hysteresis loops. This problem is relevant to the prediction of the coercive field, which is the maximum magnitude of an opposing magnetic field that a permanent magnet can withstand before its magnetization reverses[2, 3, 1]. The theory of micromagnetics predicts a much higher maximum value of coercivity than the values actually observed by experimental methods[1]. This discrepancy is known as *Brown's paradox*.

Two different time-scales are relevant to the physical processes described by hysteresis curves: the time-scale of variation of the external applied field and the time-scale of relaxation of the magnetization distribution towards the equilibrium configuration. For permanent magnet applications the relaxation time-scale is so much shorter that the system can be realistically considered to follow the equilibrium configuration as the external field is varied [1]. For this reason, although it would in principle be possible to employ fully-dynamical simulations based on the Landau-Lifshitz equation, it is often convenient to consider a different iterative approach where the two time-scales are decoupled. In each step of the iteration the field is assumed to be fixed and the equilibrium state for fixed conditions is computed; subsequently the external field is updated to the new value corresponding to the following step of the iteration [9]. We will refer to this method as "step-by-step" approach. At each step, the equilibrium state can be found by employing Landau-Lifshitz without the precession term [8], or by energy-minimization methods such as the method of conjugate gradients [7].

In this paper we present a novel simulation technique that can be used for the computation of hysteresis loops, and in general to quasi-static micromagnetic processes. As mentioned above, the system is assumed to be at equilibrium at all-times. However, when the external parameters are changed, a given equilibrium configuration may suddenly become unstable, an event known as bifurcation. When a bifurcation occurs, the system undergoes a rapid transition to a new equilibrium state.

We analyze the change of stability of equilibrium configurations by employing standard methods from the stability theory of classical dynamical systems. We consider the differential equation governing the evolution of the equilibrium configuration with respect to a variation of some external parameter, typically the external magnetic field applied to a permanent magnet sample. The key strength of our approach is that the governing equation automatically guarantees that the state of the system continuously follows a given equilibrium configuration for as long as possible, i.e. until a bifurcation occurs. We illustrate this novel direct approach with two simple examples computed with the micromagnetic and magnetostatic simulation framework MagTense[15].

1.2 Notation

- **Vectors, vector fields, tensors and tensor fields**

  Bold font, as in $\boldsymbol{x}$, denotes vectors. Normalized vectors are indicated with the hat, as in $\hat{\boldsymbol{x}}$. The independent variable $\boldsymbol{x}$ of a vector field $\boldsymbol{m} : \mathbb{R}^3 \to \mathbb{R}^3$ is indicated between round brackets, as in $\boldsymbol{m}(\boldsymbol{x})$. Rank-2 tensors are indicated with double underlining, as in $\underline{\underline{A}}$. The independent variable of a tensor field is indicated between round brackets, as in $\underline{\underline{A}}(\boldsymbol{x})$.

- **Functionals and operators**

  We consider scalar-valued functionals having a vector field, such as $\boldsymbol{m}(\boldsymbol{x})$, as input. We will use calligraphic font, as in $\mathcal{G}$, to denote functionals, and square brackets for the input argument, as in $\mathcal{G}[\boldsymbol{m}]$. In this context, $\mathcal{G}$ is a scalar-valued function defined over the Hilbert space $\mathbb{V}$ of square integrable vector fields over $\mathbb{R}^3$. The vector field $\boldsymbol{m}$ is thus as an element of $\mathbb{V}$, and will be referred to simply as "point".

  We will also consider operators having vector fields both as input and output arguments. The input argument of an operator is also indicated with square brackets, as in $\boldsymbol{q}[\boldsymbol{m}]$.

- **Gradient, Jacobian and Hessian**

  The gradient of a functional $\mathcal{G}[\boldsymbol{m}]$ is denoted by $\boldsymbol{\nabla}\mathcal{G}$. The Jacobian matrix of an operator $\boldsymbol{f}$ is denoted by $\underline{\underline{\mathbb{J}}}\boldsymbol{f}$ The Hessian matrix of a functional $\mathcal{G}$ is denoted by $\underline{\underline{\underline{\mathbb{H}}}}\mathcal{G}$. Each of these differential operators are with respect to the independent variables, which are all the components of the input vector field. The point of $\mathbb{V}$ at which a differential operator is evaluated is indicated by subscript. For example, if the gradient of $\mathcal{G}[\boldsymbol{m}]$ is evaluated at the point $\boldsymbol{m}^*$, we write $(\boldsymbol{\nabla}\mathcal{G})_{\boldsymbol{m}^*}$ to indicate this.

1.3 Micromagnetic free energy

The magnetic state of the micromagnetic system considered is described by the magnetization distribution $\boldsymbol{M}(\boldsymbol{x})$, where $\boldsymbol{x}$ denotes a generic point in space. It is assumed that the norm of $\boldsymbol{M}$ is predetermined. This is denoted by M_s. The magnetization can thus be written as

$$\boldsymbol{M}(\boldsymbol{x}) = M_s \boldsymbol{m}(\boldsymbol{x}) \tag{1}$$

where $\boldsymbol{m} = m_x\hat{\boldsymbol{e}}_x + m_y\hat{\boldsymbol{e}}_y + m_z\hat{\boldsymbol{e}}_z$ denotes the normalized magnetization, also called the *reduced magnetization*, which satisfies $\|\boldsymbol{m}\| = 1$.

At equilibrium, the magnetization distribution minimizes the micromagnetic free energy. The energy is expressed by a functional $\mathcal{G}$ composed of four terms [10, 11]:

$$\mathcal{G}[\boldsymbol{m}] = \mathcal{G}_{\text{exch}}[\boldsymbol{m}] + \mathcal{G}_{\text{anis}}[\boldsymbol{m}] + \mathcal{G}_{\text{ext}}[\boldsymbol{m}] + \mathcal{G}_{\text{demag}}[\boldsymbol{m}] \tag{2}$$

The four terms represent four different contributions to the total energy. All the terms are expressed as volume integrals over the magnet domain Ω of corresponding energy density functions:

- Exchange term:

$$\mathcal{G}_{\text{exch}}[\boldsymbol{m}] = \int_\Omega dV\ C_{\text{exch}} \left(\|\boldsymbol{\nabla} m_x\|^2 + \|\boldsymbol{\nabla} m_y\|^2 + \|\boldsymbol{\nabla} m_z\|^2 \right) \tag{3}$$

  where C_{exch} denotes the exchange constant.

- Anisotropy term:

$$\mathcal{G}_{\text{anis}}[\boldsymbol{m}] = \int_\Omega dV\ f_{\text{anis}}(\boldsymbol{m}) \tag{4}$$

  where f_{anis} is the anisotropy energy density which only depends on the local value of the magnetization distribution. Uni-axial anisotropy is often modeled by $f_{\text{anis}}(\boldsymbol{m}) = -K(\boldsymbol{m}\cdot\hat{\boldsymbol{e}}_K)^2$, where K is the anisotropy constant and $\hat{\boldsymbol{e}}_K$ is the unit vector pointing along the easy axis of the crystal lattice. In this case, the anisotropy energy is quadratic with respect to $\boldsymbol{m}$.

- External field term:

$$\mathcal{G}_{\text{ext}}[\boldsymbol{m}] = -\mu_0 M_s \int_\Omega dV\ (\boldsymbol{m}\cdot\boldsymbol{H}_a) \tag{5}$$

  where $\boldsymbol{H}_a$ denotes the external (or applied) field.

- Demagnetization term:

$$\mathcal{G}_{\text{demag}}[\boldsymbol{m}] = -\left(\frac{\mu_0 M_s}{2}\right) \int_\Omega dV\ (\boldsymbol{m}\cdot\boldsymbol{H}_d) \tag{6}$$

  where $\boldsymbol{H}_d$ denotes the demagnetization field, i.e. the field generated by the magnetization distribution $\boldsymbol{M}$ itself.

Note that the demagnetization field $\boldsymbol{H}_d$ depends linearly on $\boldsymbol{m}$:

$$\boldsymbol{H}_d = \boldsymbol{N}[\boldsymbol{m}] \tag{7}$$

where $\boldsymbol{N}$ is a linear operator:

$$\boldsymbol{N}[a\,\boldsymbol{m}_a + b\,\boldsymbol{m}_b] = a\,\boldsymbol{N}[\boldsymbol{m}_a] + b\,\boldsymbol{N}[\boldsymbol{m}_b] \tag{8}$$

Here $\boldsymbol{m}_a$ and $\boldsymbol{m}_b$ are two arbitrary magnetization distributions, while a and b are two arbitrary real numbers. In fact, the demagnetization field at the point $\boldsymbol{x}$ can be expressed as the following integral:

$$\boldsymbol{H}_d(\boldsymbol{x}) = \int_\Omega dV'\, \underline{\underline{N}}(\boldsymbol{x}, \boldsymbol{x}')\, \boldsymbol{m}(\boldsymbol{x}') \tag{9}$$

Moreover, the tensor field $\underline{\underline{N}}$ is symmetric[11]:

$$\underline{\underline{N}}(\boldsymbol{x}, \boldsymbol{x}') = \underline{\underline{N}}^T(\boldsymbol{x}, \boldsymbol{x}') \tag{10}$$

From the various expressions introduced above, it is clear that, as long as the anisotropy is uni-axial, the total energy is quadratic in $\boldsymbol{m}$. Therefore, the total energy $\mathcal{G}$ is expressed by the following double integral over the region Ω:

$$\mathcal{G}[\boldsymbol{m}] = \int_\Omega dV \int_\Omega dV'\, \boldsymbol{m}^T(\boldsymbol{x}) \underline{\underline{A}}(\boldsymbol{x}, \boldsymbol{x}')\, \boldsymbol{m}(\boldsymbol{x}') + \int_\Omega dV\, \boldsymbol{m}^T(\boldsymbol{x}) \boldsymbol{b}(\boldsymbol{x}). \tag{11}$$

From this point we will omit the integration domain Ω, since all the volume integrals are always performed over this domain. Because of the symmetry properties satisfied by all the four terms, the tensor field $\underline{\underline{A}}$ is also symmetric[11]:

$$\underline{\underline{A}}(\boldsymbol{x}, \boldsymbol{x}') = \underline{\underline{A}}^T(\boldsymbol{x}, \boldsymbol{x}') \tag{12}$$

The tensor field $\underline{\underline{A}}$ is composed by three different terms corresponding to the exchange, anisotropy and demagnetization terms, respectively:

$$\underline{\underline{A}}(\boldsymbol{x}, \boldsymbol{x}') = \underline{\underline{A}}_{\text{exch}}(\boldsymbol{x}, \boldsymbol{x}') + \underline{\underline{A}}_{\text{anis}}(\boldsymbol{x}, \boldsymbol{x}') + \underline{\underline{A}}_{\text{demag}}(\boldsymbol{x}, \boldsymbol{x}') \tag{13}$$

The explicit expressions for the three terms can be written in terms of the three-dimensional Dirac delta function $\delta^3(\boldsymbol{x})$:

$$\underline{\underline{A}}_{\text{exch}}(\boldsymbol{x}, \boldsymbol{x}') = C_{\text{exch}}\, \underline{\underline{1}} \int_\Omega dV'' \Big(\boldsymbol{\nabla}_{\boldsymbol{x}} \delta^3(\boldsymbol{x} - \boldsymbol{x}'') \Big) \cdot \Big(\boldsymbol{\nabla}_{\boldsymbol{x}'} \delta^3(\boldsymbol{x}' - \boldsymbol{x}'') \Big) \tag{14}$$

$$\underline{\underline{A}}_{\text{anis}}(\boldsymbol{x}, \boldsymbol{x}') = -K(\hat{\boldsymbol{e}}_K)(\hat{\boldsymbol{e}}_K)^T \delta^3(\boldsymbol{x} - \boldsymbol{x}') \tag{15}$$

$$\underline{\underline{A}}_{\text{demag}}(\boldsymbol{x}, \boldsymbol{x}') = -\left(\frac{\mu_0 M_s}{2} \right) \underline{\underline{N}}(\boldsymbol{x}, \boldsymbol{x}') \tag{16}$$

where $\underline{\underline{1}}$ denotes the 3×3 identity matrix. The vector field $\boldsymbol{b}$ is entirely determined by the external field:

$$\boldsymbol{b}(\boldsymbol{x}) = \boldsymbol{b}_{\text{ext}}(\boldsymbol{x}) = -\mu_0 M_s \boldsymbol{H}_a \tag{17}$$

2 Methods

2.1 The effective field

In order to use numerical methods, we need to transform the continuous formulation, expressed by Eq. 11, into a discretized formulation. There are many ways to approximate the original problem with a discrete problem. The treatment discussed in the present paper can be equally applied regardless of the particular choice of discretization approach.

Here we assume that the magnetization distribution is expanded over a discrete mesh over the three-dimensional space. In our implementation we use a Cartesian grid composed by N identical rectangular prisms, which we will refer to as *tiles*. The magnetization is assumed uniform over each of these tiles. With this assumption, the demagnetization field generated by each of these tiles can be calculated analytically [16]. Because of the superposition principle, the total field is the sum of the contributions from all the tiles composing the grid.

The discretization of the magnet domain Ω into rectangular prisms is illustrated in Fig. 1. Fig. 1(b) shows one prism and the magnetic flux density generated by this tile when uniformly magnetized in the y direction. Fig. 1(a) shows the subdivision of the region Ω into N identical copies of the same prism. It should be noted that, although here for the sake of simplicity we have chosen a collection of identical rectangular prisms, the methods discussed in this paper can be equally applied for any discrete mesh composed by non-identical tiles of arbitrary shape[19]. The only requirement is to be able to compute the demagnetization field associated with any discretized magnetization distribution defined over the mesh.

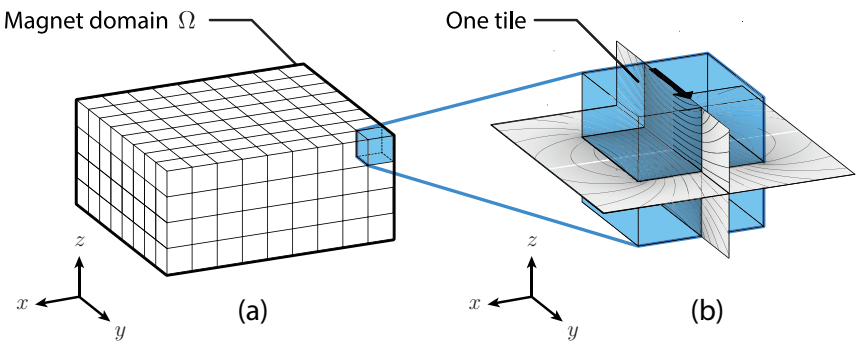

Figure 1: (a) Illustration of the discretized grid subdividing the magnet domain Ω. The demagnetization field and the other terms of the effective field are computed by summing the contributions from all the tiles. (b) The magnetic flux density generated by one tile can be calculated analytically. As an example, Fig. 1 shows the field generated by the tile when it is magnetized along the y direction.

We will denote by the symbol, $\boldsymbol{m}$, the $3N$ elements array of the expansion of $\boldsymbol{m}(\boldsymbol{x})$ over the N-tiles grid. The discretized vector field $\boldsymbol{m}$ is an element of the vector space $\mathbb{R}^{3N}$. Then using collective indexes, the j^{th} component of the $3N$ vector is denoted by m_j. This corresponds to one of the 3 components of the magnetization vector associated with a given point of the

grid. Similarly, we denote by A_{kj} one entry of the expansion of the tensor field $\underline{\underline{A}}$ over the N-tiles grid, and by b_k one entry of the vector field $\boldsymbol{b}$. The discretized expression of the energy functional $\mathcal{G}$ is thus given by:

$$\mathcal{G}[\boldsymbol{m}] = \sum_k \sum_j m_k A_{kj} m_j + \sum_k m_k b_k \tag{18}$$

All the summations are performed over the $3N$ components of the discretized arrays. It is conventional to employ a variational approach, and to express the first variation of the functional $\mathcal{G}$ in terms of the so-called *effective field* [10, 11]. In the continuous formulation, the effective field is expressed as:

$$\boldsymbol{H}_{\text{eff}} = \left(\frac{2C_{\text{exch}}}{\mu_0 M_s}\right)\left(\partial_x^2 \boldsymbol{m} + \partial_y^2 \boldsymbol{m} + \partial_z^2 \boldsymbol{m}\right) - \left(\frac{1}{\mu_0 M_s}\right)\frac{\partial f_{\text{anis}}}{\partial \boldsymbol{m}} + \boldsymbol{H}_a + \boldsymbol{H}_d \tag{19}$$

Except for a scale factor $(\mu_0 M_s)^{-1}$ which for simplicity we will neglect here, the discretized effective field $\boldsymbol{H}_{\text{eff}}$ is the negative of the gradient of $\mathcal{G}$ with respect to $\boldsymbol{m}$ [12]:

$$\boldsymbol{H}_{\text{eff}}[\boldsymbol{m}] = -\left(\boldsymbol{\nabla}\mathcal{G}\right)_{\boldsymbol{m}} \tag{20}$$

Since $\mathcal{G}[\boldsymbol{m}]$ is quadratic, its gradient $\boldsymbol{H}_{\text{eff}}$ is linear with respect to $\boldsymbol{m}$:

$$\left(\frac{\partial \mathcal{G}}{\partial m_k}\right)_{\boldsymbol{m}} = 2\sum_j A_{kj} m_j + b_k \tag{21}$$

2.2 Normalization condition and Landau-Lifshitz equation

The vector field $\boldsymbol{m}$ must be normalized at any point. We thus introduce the point-wise normalization operator $\boldsymbol{q}$:

$$\boldsymbol{q}[\boldsymbol{m}] = \frac{\boldsymbol{m}(\boldsymbol{x})}{\|\boldsymbol{m}(\boldsymbol{x})\|}, \quad \forall \boldsymbol{x} \tag{22}$$

Our problem is thus to minimize the following composite functional:

$$\mathcal{H}\big[\boldsymbol{m}\big] = \mathcal{G}\big[\boldsymbol{q}[\boldsymbol{m}]\big] \tag{23}$$

Clearly, the functional $\mathcal{H}$ is not quadratic with respect to $\boldsymbol{m}$. The gradient of $\mathcal{H}$ can be calculated from the gradient of $\mathcal{G}$ and the Jacobian of $\boldsymbol{q}$. The Jacobian of $\boldsymbol{q}$ is the operator consisting of taking the vector product with $\boldsymbol{m}$ twice, and dividing by $-\|\boldsymbol{m}\|^3$. Denoting by $\left(\underline{\underline{\mathbb{J}}}\,\boldsymbol{q}\right)_{\boldsymbol{m}} \boldsymbol{v}$ the Jacobian matrix evaluated at $\boldsymbol{m} \in \mathbb{V}$ and multiplied by an arbitrary vector field $\boldsymbol{v}$ we have:

$$\left(\underline{\underline{\mathbb{J}}}\,\boldsymbol{q}\right)_{\boldsymbol{m}} \boldsymbol{v} = -\left(\frac{1}{\|\boldsymbol{m}\|^3}\right)\boldsymbol{m}(\boldsymbol{x}) \times \boldsymbol{m}(\boldsymbol{x}) \times \boldsymbol{v}(\boldsymbol{x}), \quad \forall \boldsymbol{x} \tag{24}$$

The gradient of the composition $\mathcal{H}\big[\boldsymbol{m}\big] = \mathcal{G}\big[\boldsymbol{q}[\boldsymbol{m}]\big]$ is the Jacobian of $\boldsymbol{q}$ multiplied by the gradient of $\mathcal{G}[\boldsymbol{q}]$ evaluated at $\boldsymbol{q}[\boldsymbol{m}]$:

$$\left(\frac{\partial \mathcal{H}}{\partial m_j}\right)_{\boldsymbol{m}} = \sum_k \left(\frac{\partial q_k}{\partial m_j}\right)_{\boldsymbol{m}} \left(\frac{\partial \mathcal{G}}{\partial q_k}\right)_{\boldsymbol{q}[\boldsymbol{m}]} \tag{25}$$

As a vector equation the previous relation is written as:

$$\left(\nabla_{\boldsymbol{m}} \mathcal{H}\right)_{\boldsymbol{m}} = \left(\underline{\underline{\mathbb{J}}}\,\boldsymbol{q}\right)_{\boldsymbol{m}} \left(\boldsymbol{\nabla}\mathcal{G}\right)_{\boldsymbol{q}[\boldsymbol{m}]} = \left(\frac{1}{\|\boldsymbol{m}\|^3}\right)\boldsymbol{m} \times \boldsymbol{m} \times \boldsymbol{H}_{\text{eff}}[\hat{\boldsymbol{m}}] \tag{26}$$

If we evaluate the gradient of $\mathcal{H}$ at a point of $\mathbb{V}$ satisfying the constraint, i.e. $\boldsymbol{m} = \hat{\boldsymbol{m}}$, we can simplify the previous expression:

$$(\boldsymbol{\nabla}\mathcal{H})_{\hat{\boldsymbol{m}}} = \hat{\boldsymbol{m}} \times \hat{\boldsymbol{m}} \times \boldsymbol{H}_{\text{eff}}[\hat{\boldsymbol{m}}] \tag{27}$$

This is one way to see that the dissipative term of the Landau-Lifshitz equation [11] is equivalent to a gradient descent for the composition $\mathcal{H}$, or equivalently a gradient descent for $\mathcal{G}$ that satisfies the point-wise constraint[10]. We will assume that magnetization distribution $\boldsymbol{m}$ is governed by the Landau-Lifshitz equation. Since the subject of this work is determining the equilibrium configurations, we only include the dissipative term, i.e. we do not consider the precessional term. The governing equation is thus expressed as:

$$\frac{d}{dt}\boldsymbol{m} = \boldsymbol{f}[\boldsymbol{m}] = -\alpha\, \boldsymbol{m} \times (\boldsymbol{m} \times \boldsymbol{H}_{\text{eff}}[\boldsymbol{m}]) \tag{28}$$

where $\alpha \in \mathbb{R}_{>0}$ is the damping coefficient. The reason for the minus sign in the time-evolution Eq. 28, is that the equation should lead the state of the system towards energy *minima*. The initial state is normalized at each point $\boldsymbol{x}$:

$$\boldsymbol{m}(t=0) = \hat{\boldsymbol{m}}(t=0) \tag{29}$$

In this case the norm is preserved by Eq. 28. For now, we also assume that $\boldsymbol{f}$ does not depend explicitly on the time t. An equilibrium state $\boldsymbol{m}^*$ is invariant with respect to Eq. 28:

$$\frac{d}{dt}\boldsymbol{m}^* = \boldsymbol{f}[\boldsymbol{m}^*] = \boldsymbol{0} \tag{30}$$

From the definition of $\boldsymbol{f}$ we see that Eq. 30 requires the effective field to be parallel to the magnetization $\boldsymbol{m}$ at each point in the grid. An equilibrium point is called stable if the system is guaranteed to return to the same equilibrium configuration when the magnetization distribution is subject to a sufficiently small perturbation. In the context of non-linear equations such an equilibrium point is sometimes called metastable, since it is not guaranteed to be unique, nor to be the global minimum of the micromagnetic energy [4].

2.3 Hysteresis loops: conventional calculation approaches

Here we focus on the phenomenon of magnetic hysteresis. This phenomenon can be observed when multiple equilibrium configurations exist for the same conditions. We consider the case of an external uniform field $\boldsymbol{H}_a$ applied along a given direction $\hat{\boldsymbol{e}}_a$. We evaluate the total magnetic moment of the system along this direction. The normalized total magnetic moment in the direction $\hat{\boldsymbol{e}}_a$ is denoted by $\hat{m}_a$ and defined as:

$$\hat{m}_a = \left(\frac{1}{V}\right) \int_\Omega dV\, \hat{\boldsymbol{e}}_a \cdot \boldsymbol{m}(\boldsymbol{x}) \tag{31}$$

where V is the total volume of the magnet domain Ω. The magnitude H_a of the applied field is varied over time, and spans the interval $[-H_{\max}, +H_{\max}]$.

We assume that the rate of variation of the external field is much lower than the rate of convergence to equilibrium, and thus the process is quasistatic. In these conditions the system will remain on the same equilibrium point as the external field is varied. However, there might be several distinct stable equilibrium points compatible with the same set of external conditions. Moreover, as the external field is varied, a given equilibrium point might become unstable or disappear. As discussed in the next section, this event is called a bifurcation [13]. When a bifurcation occurs the system will undergo a transition to the energetically closest equilibrium

configuration. In other words the energy landscapes evolves in such a way that the system falls into the basin of attraction of a different equilibrium point.

There are two conventional approaches to calculate hysteresis loops i.e. different from the method proposed here. We will refer to the two approaches as the *dynamic approach* and the *step-by-step approach*, respectively.

- In the dynamic approach, the field variation and the convergence to equilibrium happen simultaneously. The state of the system evolves according to Eq. 28, with an explicitly time-dependent effective field. In order to reproduce the quasistatic behavior, the damping coefficient α must be very large with respect to the rate of variation of the external field. As long as α is sufficiently large, the system should remain at equilibrium while the external field changes.
- In the step-by-step approach the evolution is still governed by Eq. 28, but the external conditions are fixed. When the equilibrium point is reached, the external field is instantaneously varied by a small amount, and the system is then allowed to converge to the new equilibrium state. As long as the field variation between consecutive steps is sufficiently small, this computation scheme should correctly reproduce the quasistatic regime.

It is thus clear in both cases, the validity of the approach depends on a proper choice of the simulation parameters: the value of α for the dynamic approach, and the step-size for the step-by-step approach.

2.4 Bifurcations and eigenvalues

A bifurcation occurs when an equilibrium point disappears or becomes unstable. This is typically seen in e.g. calculation of hysteresis loops when the magnetization discontinuously jumps from one magnetization to another, although bifurcations can also be continuous transitions, as will be shown subsequently.

When the external field is varied, the function $\boldsymbol{f}$ appearing in Eq. 28 changes accordingly. In order to highlight the mechanism of bifurcations, we assume that the external field is parameterized by a real scalar number σ. We thus write the equation of motion in a form that highlights the explicit dependence of $\boldsymbol{f}$ on σ:

$$\frac{d}{dt}\boldsymbol{m} = \boldsymbol{f}[\boldsymbol{m}; \sigma] \tag{32}$$

For a time-continuous dynamical system, the signature of a bifurcation is the vanishing of the real part of one of the eigenvalues of the Jacobian matrix of $\boldsymbol{f}$. For the micromagnetics problem $\boldsymbol{f}$ is proportional to the gradient of the composite functional $\mathcal{H}$ from Eqs. 27 and 28:

$$\boldsymbol{f} = -\alpha\left(\boldsymbol{\nabla}\mathcal{H}\right) \quad \Rightarrow \quad \underline{\underline{\mathbb{J}}}\,\boldsymbol{f} = -\alpha\left(\underline{\underline{\mathbb{H}}}\,\mathcal{H}\right) \tag{33}$$

where $\underline{\underline{\mathbb{H}}}\,\mathcal{H}$ denotes the Hessian of $\mathcal{H}[\boldsymbol{m}] = \mathcal{G}[\boldsymbol{q}[\boldsymbol{m}]]$ with respect to $\boldsymbol{m}$. We can calculate the Hessian analytically by applying Faà di Bruno's formula for the second derivatives of multivariate composite functions (see the Appendix):

$$\left(\frac{\partial^2\mathcal{H}}{\partial m_i \partial m_j}\right)_{\boldsymbol{m}} = \sum_k \left(\frac{\partial\mathcal{G}}{\partial q_k}\right)_{\boldsymbol{q}[\boldsymbol{m}]} \left(\frac{\partial^2 q_k}{\partial m_i \partial m_j}\right)_{\boldsymbol{m}} + \sum_k \sum_\ell \left(\frac{\partial^2\mathcal{G}}{\partial q_k \partial q_\ell}\right)_{\boldsymbol{q}[\boldsymbol{m}]} \left(\frac{\partial q_k}{\partial m_i}\right)_{\boldsymbol{m}} \left(\frac{\partial q_\ell}{\partial m_j}\right)_{\boldsymbol{m}} \tag{34}$$

As we see from the right-hand side of the previous equation, the Hessian of $\mathcal{H}$ is composed of two terms. The first term depends on the effective field, i.e. on the first derivatives of $\mathcal{G}$, and on the second derivatives of $\boldsymbol{q}$. The second term depends on the Hessian of $\mathcal{G}$, which is the double of the matrix A appearing in Eq. 18, and on the first derivatives of $\boldsymbol{q}$.

Since the first order derivatives of $\mathcal{H}$ are zero at an equilibrium point, the next-order approximation (i.e. quadratic) is the simplest description of the local behavior of $\mathcal{H}$ around the equilibrium point. Since $\mathcal{G}$ is a quadratic functional, the Hessian matrix of $\mathcal{G}$ is fixed, i.e. it does not depend on $\boldsymbol{m}$. In other words the matrix $\underline{\underline{\mathbb{H}}}\mathcal{G}$ is an *exact* description of the behavior of $\mathcal{G}$ *everywhere*. On the contrary, the Hessian of $\mathcal{H}$, which depends on $\boldsymbol{m}$, is only an *approximate* description of the behavior of $\mathcal{H}$ *in the vicinity* of an equilibrium point.

As mentioned above, bifurcations are identified by the studying the eigenvalues of $\underline{\underline{\mathbb{H}}}\mathcal{H}$. Because of Schwarz's theorem, any Hessian matrix is symmetric, and therefore all the eigenvalues are purely real numbers. Before the bifurcation occurs the equilibrium point is assumed to be stable, and the eigenvalues are thus negative. Therefore, we can detect a bifurcation by considering the largest eigenvalue, denoted by $\lambda_{\max}$. It is not necessary to compute all the eigenvalues: there are efficient algorithms for calculating directly the largest eigenvalue. When a bifurcation occurs at $\sigma = \sigma^{\bigstar}$, the largest eigenvalue $\lambda_{\max}$ converges to 0^- as σ approaches $\sigma^{\bigstar}$.

2.5 Direct method

We developed an alternative *direct* method for simulating quasistatic processes. The approach considers the differential equation obeyed by the equilibrium state $\boldsymbol{m}^*$, with respect to the independent variable σ.

An equilibrium state $\boldsymbol{m}^*$ satisfies the equation $\frac{d}{dt}\boldsymbol{m}^* = \boldsymbol{0}$, which is written as:

$$\boldsymbol{f}[\boldsymbol{m}^*(\sigma); \sigma] = \boldsymbol{0} \tag{35}$$

As highlighted by the previous expression, the equilibrium state $\boldsymbol{m}^*$ depends on σ. The parameter σ is varied over time quasi-statically, i.e. at a much slower rate with respect to the rate of convergence of $\boldsymbol{m}$ towards $\boldsymbol{m}^*(\sigma)$. We can thus write the implicit ordinary differential equation, with independent variable σ, which governs the evolution of $\boldsymbol{m}^*(\sigma)$. By taking the derivative with respect to σ on both sides of Eq. 35, we obtain the following equation:

$$\frac{d}{d\sigma}\boldsymbol{f}[\boldsymbol{m}^*(\sigma); \sigma] = \boldsymbol{0} \tag{36}$$

The equation can be written as:

$$\boldsymbol{f}^*\left[\boldsymbol{m}^*, \frac{d}{d\sigma}\boldsymbol{m}^*; \sigma\right] = \boldsymbol{0} \tag{37}$$

Where $\boldsymbol{f}^*$ is given by:

$$\boldsymbol{f}^* = \left(\underline{\underline{\mathbb{J}}}\boldsymbol{f}\right)\frac{d}{d\sigma}\boldsymbol{m}^* + \frac{\partial}{\partial\sigma}\boldsymbol{f} = 0 \tag{38}$$

In this form the differential equation is implicit. We can transform it into an explicit equation by solving $\boldsymbol{f}^*$ with respect to $\frac{d}{d\sigma}\boldsymbol{m}^*$:

$$\frac{d}{d\sigma}\boldsymbol{m}^* = -\left(\underline{\underline{\mathbb{J}}}\boldsymbol{f}\right)^{-1}\frac{\partial}{\partial\sigma}\boldsymbol{f} \tag{39}$$

The geometrical interpretation of the equation $\frac{d}{d\sigma}\boldsymbol{f} = \boldsymbol{0}$ is thus that the gradient of $\mathcal{H}$ does not change as σ is varying: since we are following the equilibrium point, the gradient must remain zero. In particular, the first term on the right-hand side of Eq. 38 corresponds to the variation of the gradient due to the shift $d\boldsymbol{m}^*$, while the second term corresponds to the explicit variation of the gradient due to change of σ. The equation prescribes that the two variations must compensate each other.

2.6 Change of basis

It is important to realize that the matrix $\underline{\underline{\mathbb{J}}}\boldsymbol{f}$ is actually singular: because of the normalization operator $\boldsymbol{q}$, a variation $d\boldsymbol{m}^*$ that would increase the norm of $\boldsymbol{m}^*$ in a point of the grid has no effect. In other words, a shift $d\boldsymbol{m}^*$ produces the same variation of the gradient $\boldsymbol{\nabla}\mathcal{H}$ regardless of the component of $d\boldsymbol{m}^*$ that is parallel to $\boldsymbol{m}^*$ at a given point $\boldsymbol{x}$. There are thus N eigenvalues that are equal to zero: one for each tile of the grid. This implies that $\frac{d}{d\sigma}\boldsymbol{m}^*$ is not uniquely defined by Eq. 37.

We can work around this issue by performing a suitable change of basis. For each of the N tiles $\boldsymbol{x}_i$ we consider three normalized orthogonal vectors: $\hat{\boldsymbol{e}}_1(\boldsymbol{x}_i)$, $\hat{\boldsymbol{e}}_2(\boldsymbol{x}_i)$, and $\hat{\boldsymbol{e}}_3(\boldsymbol{x}_i)$. One of the three vectors is equal to the magnetization vector in that tile: $\hat{\boldsymbol{e}}_1(\boldsymbol{x}_i) \equiv \boldsymbol{m}(\boldsymbol{x}_i)$. The second vector can be calculated by taking the cross product between $\hat{\boldsymbol{e}}_1$ and an arbitrary normalized vector. The third vector is defined as $\hat{\boldsymbol{e}}_3 = \hat{\boldsymbol{e}}_1 \times \hat{\boldsymbol{e}}_2$.

We thus have 3 orthogonal unit vectors for each of the N tiles. From these $3N$ vectors we can build a new basis for the space $\mathbb{R}^{3N}$ of all the vector fields over the grid. After expressing Eq. 37 over the new basis, we do not consider the components corresponding to the vectors $\hat{\boldsymbol{e}}_1(\boldsymbol{x}_i)$, since these correspond to the N eigenvalues that are equal to zero. We thus have a reduced $2N \times 2N$ system of equations which is not anymore singular:

$$\left(\tilde{\underline{\underline{\mathbb{J}}}}\tilde{\boldsymbol{f}}\right)\frac{d}{d\sigma}\tilde{\boldsymbol{m}}^* + \frac{\partial}{\partial\sigma}\tilde{\boldsymbol{f}} = \boldsymbol{0} \tag{40}$$

where the symbol $\tilde{}$ indicates the expansion over the reduced $2N$-elements basis. We compute the solution of the linear system over this basis, and we then set to zero the components of the solution corresponding to the vectors $\hat{\boldsymbol{e}}_1(\boldsymbol{x}_i)$. Finally, we perform the inverse change of basis to obtain the expansion of $\frac{d}{d\sigma}\boldsymbol{m}^*$ over the original basis. This procedure automatically ensures that the derivative $\frac{d}{d\sigma}\boldsymbol{m}^*$ is normal to the magnetization $\boldsymbol{m}$ at each point, and the norm is thus preserved. It is worth mentioning that since the change of basis is point-wise the corresponding matrix is sparse.

2.7 Implementation

The numerical simulations have been performed with the micromagnetic and magnetostatic simulation framework MagTense[15].

As mentioned in Sec. 2.1, we discretize the original continuous problem by expanding the vector fields over a Cartesian grid composed of N tiles. For simplicity all the tiles are identical rectangular blocks, for which the analytical expression of the demagnetization tensor is known [16, 17]. To obtain the expansion over the grid of the total demagnetization field $\boldsymbol{H}_d$ we have to sum over the contributions from all the tiles. The discretized form of Eq. 9 is thus given by the following expression:

$$(H_d)_k = \sum_j N_{kj} m_j \tag{41}$$

The $3N \times 3N$ matrix $\underline{\underline{N}}$ is entirely determined by the geometry and directly proportional to M_s. For this reason, it is only necessary to compute $\underline{\underline{N}}$ once, at the beginning of the simulation. As we see from Eq. 19, the effective field contribution due to the exchange interaction involves differential operators with respect to the position[10, 11]. We employ central finite-difference schemes for the discretization of these differential operators. The implementation of the anisotropy term shown in Eq. 15 is straightforward for the case of uni-axial anisotropy. The matrix $\underline{\underline{A}}$ appearing in Eq. 21 is thus constructed from these three terms: demagnetization, exchange interaction, and anisotropy. As can be seen from Eq. 17, the vector field $\boldsymbol{b}$ is entirely determined by the applied field $\boldsymbol{H}_a$.

The differential equations described by Eq. 28 or Eq. 37 are then integrated using the built-in Matlab function `ode45`. The algorithm employed by this solver is based on an explicit Runge-Kutta (4,5) formula [14]. For the step-by-step approach, we also need a criterion to establish whether a given configuration $\boldsymbol{m}$ has reached the equilibrium or not. Denoting by $\dot{m}_i$ the i^{th} component of the expansion of $\frac{d}{dt}\boldsymbol{m}$, we consider the normalized rate of variation δ:

$$\delta = \left(\frac{1}{N} \sum_i \left| \frac{\dot{m}_i}{\alpha} \right|^2 \right)^{1/2} \tag{42}$$

Since $\dot{m}_i$ is divided by α, the value of δ does not depend on the damping coefficient. When δ is below a given threshold, the equilibrium configuration has been reached and the iteration can proceed to the following step.

For the direct approach the simulation can only be carried on until a bifurcation is reached. When the largest eigenvalue $\lambda_{\max}$ reaches zero the computation must be interrupted and continued with Eq. 28 in order to simulate the transition to the new equilibrium configuration. At this point one can continue with the direct approach described by Eq. 37 until a new bifurcation is reached. Instead of actually computing $\lambda_{\max}$, we employ the built-in Matlab function `chol` to perform a Cholesky factorization of the $2N \times 2N$ matrix block $\underline{\underline{\mathbb{J}}}\tilde{\boldsymbol{f}}$ introduced in Sec. 2.6. When a bifurcation has been reached, the matrix block is singular, and not anymore negative definite. The Matlab function `chol` returns an additional output which indicates whether this situation, corresponding to $\lambda_{\max} \to 0^-$, has occurred. This alternative method for detecting bifurcations is computationally more efficient than the explicit calculation of $\lambda_{\max}$.

It should be noted that the direct method proposed here is probably more suitable for relatively small-scale problems, where the number of tiles in the grid is not too large. In fact, the direct approach is more computationally intensive than the conventional approach for large values of N: each time the value of $\boldsymbol{m}^*$ is updated, it is necessary to recompute the $2N \times 2N$ matrix block $\underline{\underline{\mathbb{J}}}\tilde{\boldsymbol{f}}$, and to solve the corresponding system of linear equations with respect to $\frac{d}{d\sigma}\tilde{\boldsymbol{m}}^*$. The comparison of the computational cost between the two methods is discussed in Sec. 3.3.

3 Results and discussion

3.1 Example 1

To illustrate the conventional dynamic and step-by-step approaches, as well as the proposed direct method, we have calculated the hysteresis loop for a thin rectangular magnetic block. The dimensions of the rectangular magnet along the Cartesian directions are $L_x = 5.5{*}10^{-6}$ m, $L_y = 1.5 * 10^{-6}$ m, and $L_z = 0.5 * 10^{-6}$ m. The saturation magnetization is $M_s = 10^6$ A/m. The exchange constant is $A_{\text{exch}} = 6 * 10^{-10}$ J/m. Moreover, it is assumed that there is no crystal anisotropy. The external field is applied along the x direction, i.e. $\hat{\boldsymbol{e}}_a = \hat{\boldsymbol{e}}_x$. The magnitude of the applied field, is indicated by H_a, and spans the interval $[-H_{\max}, +H_{\max}]$, with $\mu_0 H_{\max} = 0.1$ T.

The discrete grid is composed by 25 tiles in the x direction, 13 tiles in the y direction, and 1 tile in the z direction. This grid would probably be too coarse for the purpose of accurately simulating the physical system under consideration. However, in this work we are only interested in highlighting the mechanism of bifurcations and the direct approach introduced in Sec. 2.5. For this purpose, it it not necessary to use a very fine grid since the same features are exhibited by small-scale systems.

The hysteresis loop of $\hat{m}_a$ as function of H_a is shown in Fig. 2. Initially, the applied field magnitude is $H_a = +H_{\max}$, and the magnetization distribution is relaxed to the corresponding

equilibrium configuration starting from the fully-saturated state: $\boldsymbol{m}(\boldsymbol{x}) = \hat{\boldsymbol{e}}_x$, $\forall \boldsymbol{x}$. The thick blue line shown corresponds to the demagnetization branch of the hysteresis loop. The thin light-blue curve correspond to the opposite process, where both the field and the magnetic moment have the opposite sign. The bifurcations on the demagnetization curves are indicated by the blue circles. The transitions between distinct equilibrium states are indicated by the dotted lines. As we can see from the bifurcations labeled as 1, 2, and 5, the transitions do not always involve a drastic change of the total magnetic moment.

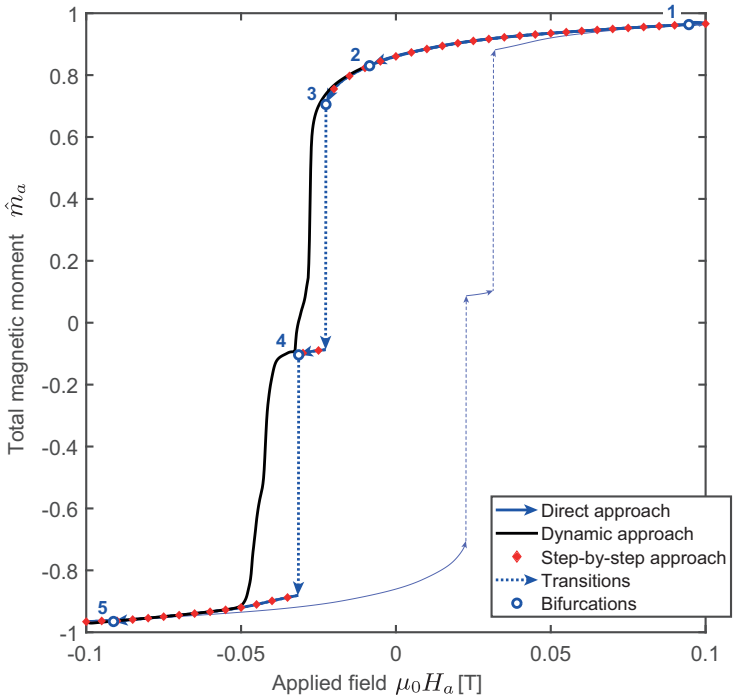

Figure 2: Magnetic hysteresis loop. The magnitude of the external field along the direction $\hat{\boldsymbol{e}}_a$ corresponds to the horizontal axis, and the normalized total magnetic moment along that direction corresponds to the vertical axis. The bifurcations of the demagnetization curve are indicated by the blue circles. The black curve, calculated with the dynamic approach, does not immediately converge to the new equilibrium after the 3$^{\text{rd}}$ and 4$^{\text{th}}$ bifurcations. The results computed with the step-by-step approach are shown as red diamonds.

For this example, the independent variable σ of the direct equation 37 is simply equal to the applied field magnitude H_a. As long as the steps-size of the step-by-step approach is small enough, the direct approach reproduces exactly the same results as the direct method, thus confirming the validity of the new method. The results obtained with the step-by-step method correspond to the red diamonds shown in Fig. 2 and are precisely overlapped with the thick blue-curve computed by the direct method proposed here.

The black curve has been calculated using the dynamic approach. As can be noticed, after a bifurcation the dynamic method does not immediately converge to the new equilibrium point.

This discrepancy indicates that a higher value of α would have been necessary in order to obtain a more precise result. For the example considered here the step-by-step method completely reproduces the correct result. However, the step-by-step method is not guaranteed to follow a given equilibrium configuration until it vanishes: with this method the system might undergo a transition to a different equilibrium even in absence of a bifurcation.

It is important to stress that the process represented by the demagnetization curve shown in Fig. 2 is irreversible, since it involves several transitions to new equilibrium configurations. Therefore, if the system undergoes the reverse process after reaching the final state, it will not return on the same curve, but on the reverse curve which in Fig. 2 is plotted in light-blue. Similarly, by reversing the process from the intermediate equilibrium state we would obtain minor hysteresis loops, which are an evidence that the process is memory-dependent, i.e. irreversible.

The magnetization distributions shown in Fig. 3 correspond to different points on the demagnetization branch of the hysteresis loop. Fig. 3(a) and Fig. 3(d) correspond to the initial and final states, respectively, i.e. to $H_a = +H_{\max}$ and $H_a = -H_{\max}$. Fig. 3(b) correspond to the state before the bifurcation labeled as 3 in Fig. 2, and Fig. 3(c) correspond to the state after the transition. During this sudden transition, occurring at $H_a = -0.226 H_{\max}$, the magnetization distribution undergoes a drastic change.

The top panel of Fig. 4 shows the evolution of the eigenvalues as the applied field H_a is reversed from $+H_{\max}$ to $-H_{\max}$ for the same example considered in Fig. 3 and Fig. 2. The largest eigenvalue is plotted as a thick blue curve. The bifurcations are indicated by the black vertical lines. We notice that $\lambda_{\max}$ converges to 0^- as H_a approaches a bifurcation from the right. In order to quantify the variation of $\boldsymbol{m}$ between two consecutive steps, we introduce the quantity Δ, defined as:

$$\Delta = \left(\frac{1}{3N} \sum_i \left| m_i^{(k+1)} - m_i^{(k)} \right|^2 \right)^{1/2} \tag{43}$$

where $m_i^{(k)}$ is the i^{th} component of the magnetization distribution at the k^{th} step of the iteration. The bottom panel of Fig. 4 shows the behavior of Δ as the applied field is reversed. Again, the bifurcations are indicated by the black vertical lines. As we can notice, when a bifurcation occurs the magnetization distribution undergoes a sudden change. However, as we can see from the 1^{st}, 2^{nd}, and 5^{th} bifurcations of Fig. 2, these sudden transitions do not always correspond to a significant variation of the total magnetic moment.

3.2 Example 2

We now consider a completely reversible process which does not exhibit any bifurcation. All the parameters are the same as in the previous example, except that the maximum magnitude of the applied field is $\mu_0 H_a = 0.5$ T, and that the field is varied according to the following equation:

$$\boldsymbol{H}_a = H_a \cos(\sigma)\hat{\boldsymbol{e}}_x + H_a \sin(\sigma)\hat{\boldsymbol{e}}_y = H_a \hat{\boldsymbol{e}}_a(\sigma) \tag{44}$$

The magnitude of the applied field is thus constant, and the direction $\hat{\boldsymbol{e}}_a$ rotates around the z axis by the angle $\sigma \in [0, 180^\circ]$. The results are plotted as function of σ in Fig. 5. Due to the large field magnitude H_a, the process leading from the initial to the final equilibrium states is completely reversible, i.e. it does not involve bifurcations. In fact, as we can notice from the bottom panel of Fig. 5, the eigenvalue $\lambda_{\max}$ is always strictly smaller than zero. Since the process is completely reversible, and the initial and final states are mirror symmetric, the curves $\lambda_k(\sigma)$ are symmetric with respect to the middle point $\sigma = 90^\circ$, and periodic with period 180°. On the contrary, the curves $\lambda_k(H_a)$ shown in the top panel of Fig. 4 are not symmetric with respect to the middle point $H_a = 0$. The top panel of Fig. 5 shows the component of the

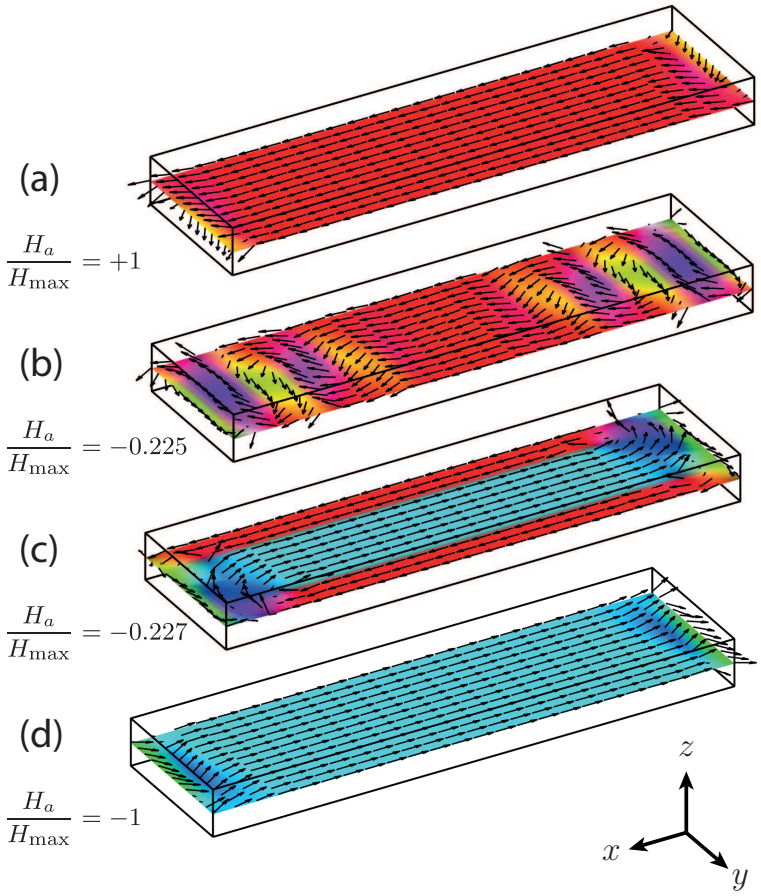

Figure 3: Examples of equilibrium magnetization distributions over a thin rectangular magnet, with an external field applied along the x direction. The color indicates the direction of the magnetization vector in that point of the magnet. The magnitude of the field along the x direction, i.e. H_a, decreases from (a) to (d), from the maximum $\mu_0 H_a = +0.1$ T to the minimum $\mu_0 H_a = -0.1$ T.

total magnetic moment along the directions $\hat{\boldsymbol{e}}_x$, $\hat{\boldsymbol{e}}_y$, and $\hat{\boldsymbol{e}}_a$. Because of the large applied field magnitude, the parallel component $\hat{m}_a$ is very close to 1 for all values of σ. However, since the lengths of the sample along the x and y directions are different, the curves $m_x(\sigma)$ and $m_y(\sigma)$ are qualitatively different: the sample is more easily magnetized along the x direction than the y direction.

Here we only considered examples where the only quantity that explicitly depends on the parameter σ is the applied field $\boldsymbol{H}_a$. However, it is important to stress that the direct method can equally be applied to compute the variation of the equilibrium state $\boldsymbol{m}^*$ with respect to any scalar variable parameterizing the governing equations. For example, we could use the direct approach to compute the evolution of $\boldsymbol{m}^*$ as function of the exchange constant A, or the saturation magnetization M_s.

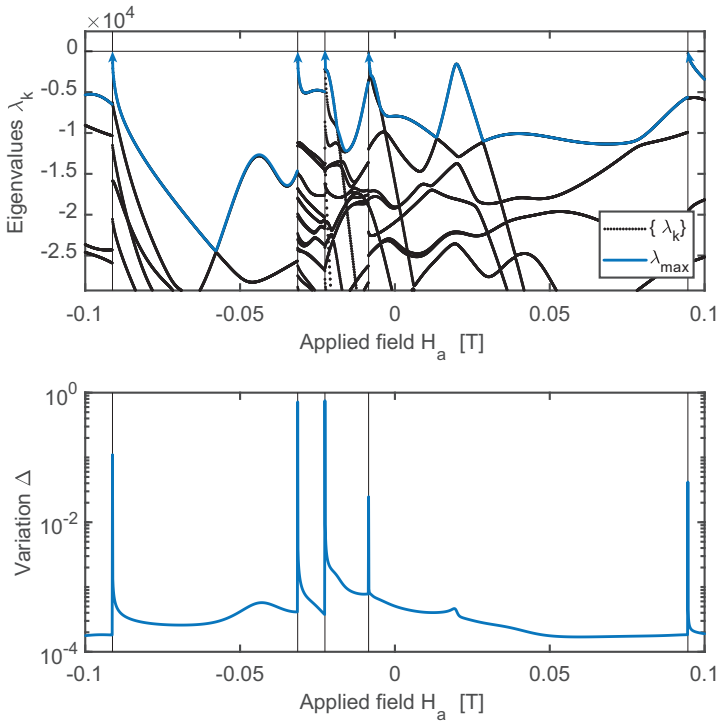

Figure 4: Top panel: eigenvalues as function of the applied field H_a. The field is decreased from $+H_{\max}$ to $-H_{\max}$. The largest eigenvalue, corresponding to the blue curve, goes to 0^- as H_a approaches a bifurcation from the right. Bottom panel: variation of the magnetization distribution $\boldsymbol{m}$ quantified by the parameter Δ defined in Eq. 43. During a bifurcation $\boldsymbol{m}$ undergoes a rapid change.

3.3 Computational cost

It is instructive to compare the computational cost of the direct approach with that of the step-by-step approach. For this purpose we performed a set of simulations on a micromagnetism problem similar to the second example discussed in Sec. 3.2, except that the magnitude of the applied field is $\mu_0 H_a = 1$ T. The reason for this difference is that increasing the field magnitude results in faster convergence, and this makes it feasible to perform a large number of simulations as required to investigate the dependence of the computational cost on the relevant parameters. The computations have been carried out on a HP Zbook with processor Intel(R) Core(TM) i7-7820HQ CPU @2.9GHz 2.90 GHz and 32 GB of RAM.

In these simulations we consider the dependence on the number of steps K at which the solution is evaluated. For the step-by-step approach, this number has a significant impact on the total computational time. On the contrary, for the direct method K does not considerably affect the computational efficiency since the number of steps at which the solution is evaluated is not necessarily equal to the the number of steps used by the solver to integrate the differential equation. This is determined by the intrinsic stability characteristics of the equation under

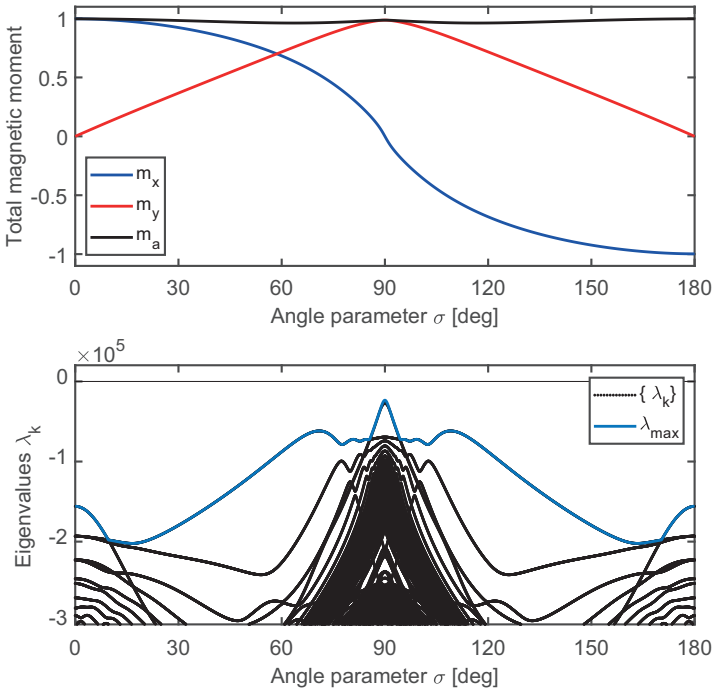

Figure 5: Top panel: total magnetic moment along different directions as function of the angle parameter σ, which controls the direction of the applied field according to Eq. 44. Because of the large field magnitude, the magnetic moment $\hat{m}_a$ along the direction of the applied field is always very close to 1. However, since the magnet has different lengths along the x and y direction, the $m_x(\sigma)$ curve and $m_y(\sigma)$ curve are different. Bottom panel: evolution of the eigenvalues as σ is varied. Since there are no bifurcations, all the eigenvalues are strictly negative.

consideration. In our implementation, employing the Matlab function `ode45`, the number of steps internally used for the integration is determined automatically by the function `ode45`.

The results are shown in Fig. 6a. In both the top and bottom panels, the horizontal axis corresponds to K. In the top panel the vertical axis corresponds to the total computation time T expressed in seconds. We consider two different discretization grids. The square markers correspond to a grid composed by 25 tiles in the x direction, 13 tiles in the y direction, and 1 tile in the z direction, for a total of $N = 325$ tiles. The diamond markers correspond to a grid composed by 27 tiles in the x direction, 15 tiles in the y direction, and 1 tile in the z direction, for a total of $N = 405$ tiles. The results computed with the step-by-step approach are shown in red, and the results computed with the direct approach are shown in blue. As a visual aid, we fitted the computational time as function of N with a polynomial function. For the step-by-step approach we used a 1^{st} degree (linear) fit, and for the direct approach we used a 0^{th} degree (constant) fit. In fact, while for the step-by-step approach the computation time T is approximately proportional to the number of steps K, for the direct approach T is nearly independent of K, for the reason explained above. Therefore, when a large number of

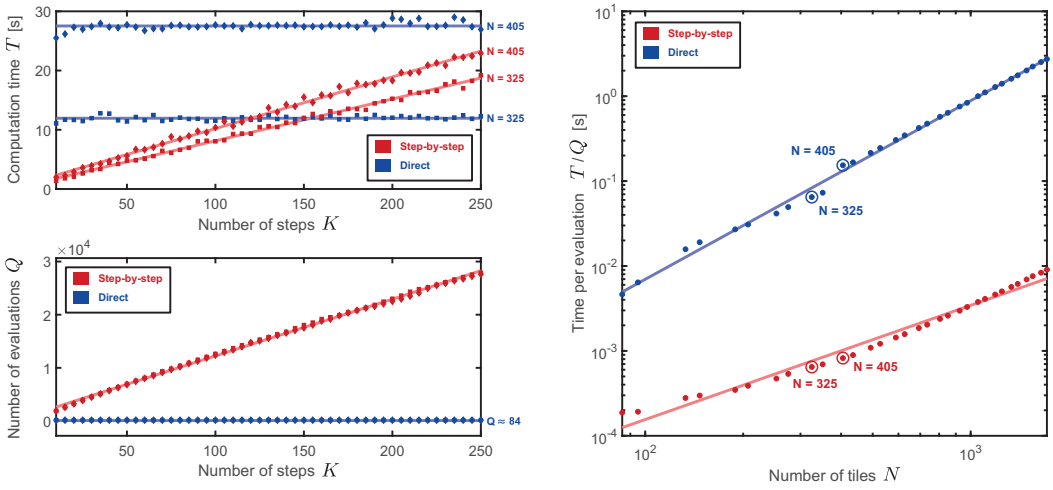

(a) (b)

Figure 6: (a) top panel: computation time T as function of the number of steps K at which the solution is evaluated. The square and diamond markers correspond to different number of tiles in the discretization grid, i.e. $N = 325$ and $N = 405$, respectively. (a) bottom panel: number of evaluations of the derivative as function of K. As can be seen, the number of tiles N has little effect on the number of evaluations Q. For the step-by-step approach both T and Q depend linearly on K, whereas for the direct approach T and Q do not depend on K. (b): computation time for each evaluation of the derivative plotted as function of the number of tiles N. For the direct approach T/Q is larger and it increases faster with increasing N, when compared to the step-by-step approach.

evaluation steps K is required, the direct method is computationally more efficient, and vice versa. As can be seen, the number of tiles N has a substantial effect on the computational time.

In the bottom panel of Fig. 6a the vertical axis corresponds to the number of evaluations Q of the derivative with respect to the integration variable (i.e. time t for the step-by-step approach, and σ for the direct approach). These results correspond to the same set of simulations of the results shown in the top panel. The value of Q is determined by the internal number of steps used by the solver for integrating the differential equation. For the step-by-step approach Q is almost exactly proportional to K, whereas for the direct approach Q does not depend on K. In both cases, the number of evaluations Q is not affected by the number of tiles N. In fact, for each of the two approaches the two data-sets corresponding to $N = 325$ and $N = 405$ are almost perfectly overlapped to each other.

This observation suggests that the two approaches must be characterized by a very different dependence on N of the computation time required for each evaluation of the derivative. In order to investigate this dependence we performed a second set of computations. We evaluated the derivative with respect to the integration variable for a randomly generated magnetization distribution $\boldsymbol{m}^{\mathrm{rnd}}$. We repeated the process for different discretization grids corresponding to a different number of tiles N. The computation time for each evaluation, denoted by T/Q, is

plotted as function of N in Fig. 6b. For each data-point T/Q has been averaged over 1000 different random distributions $\boldsymbol{m}^{\mathrm{rnd}}$. The data-points corresponding to the values of N used for the results presented in Fig. 6a are enclosed by circles.

Both the vertical and horizontal axes are in logarithmic scale. We fitted the two data-sets, corresponding to the two approaches, with a polynomial function:

$$\frac{T}{Q} = \left(\frac{N}{n_0}\right)^{\beta} \tag{45}$$

For the step-by-step approach we obtained $\beta = 1.3455$, $n_0 = 67707\ \mathrm{s}^{-1/\beta}$, for the direct approach we obtained $\beta = 2.1042$, $n_0 = 1059\ \mathrm{s}^{-1/\beta}$. As expected, the dependence on N has a more severe impact on T/Q for the direct approach than it does for the step-by-step approach. This difference is due to the fact that for each evaluation of the derivative in the direct approach it is necessary to recompute the Hessian of $\mathcal{H}$, (which explicitly depends on $\boldsymbol{m}$), to perform a change of basis, to solve a system of linear equations, and finally to perform the inverse change of basis. However, as discussed above, the direct approach often requires much less derivative-evaluations than the step-by-step approach especially when K is large, i.e. Q is generally smaller and independent of K. Therefore, from the point of view of mere computational efficiency, the direct approach is more suitable when the number of tiles N is low with respect to the required number of steps K at which the solution is evaluated.

It should be stressed that, although the general trend is well captured by these sets of simulations, the specific results are also affected by the physical problem under consideration. Depending on the energy landscape, on how does it change as function of the external parameter σ, and the trajectory of $\boldsymbol{m}^*(\sigma)$, one method might perform better than the other one, or vice versa. Moreover, the direct method is expected to be more robust with respect to premature transitions to different equilibrium states since the underlying differential equation directly describes the evolution of an equilibrium state as function of an externally varying parameter.

It should also be noted that the polynomial scaling laws given above are not necessarily indicative of the general computational performance of the MagTense framework. Efficient computational methods to approximate the demagnetization field are currently under development, and will be discussed in an upcoming paper.

3.4 Conclusion

We introduced a direct method for calculating the evolution of the equilibrium magnetization distribution $\boldsymbol{m}^*$ with respect to the variation of a scalar parameter σ which parameterizes the governing equations. We verified the validity of this novel technique against results computed with the conventional approach, here referred to as step-by-step approach.

The main advantage of this method is that the evolution is automatically guaranteed to remain to a given equilibrium state until a bifurcation occurs. Because of this feature, the direct approach is only applicable to quasi-static processes. Therefore, the direct method provides a powerful instrument for studying the evolution of equilibrium configurations during quasi-static processes, and the occurrence of bifurcations. These investigations are especially relevant for simulating field-reversal mechanisms, and predicting the coercivity of permanent magnets, which is an active area of modern research[1].

Acknowledgment

This work was supported by the Poul Due Jensen Foundation project on Browns paradox in permanent magnets under Project 2018-016.

Appendix

The n^{th} derivative of the composite function $\mathcal{G}[\boldsymbol{q}[m]]$ is given by Faà di Bruno's formula [18]:

$$D^n\mathcal{G}[\boldsymbol{q}[m]] = \sum_{\{k_j\}\in K} \frac{n!}{k_1!\dots k_n!}(D^k\mathcal{G})_{\boldsymbol{q}[\boldsymbol{m}]}\left(\frac{D^1\boldsymbol{q}[\boldsymbol{m}]}{1!}\right)^{k_1}\dots\left(\frac{D^n\boldsymbol{q}[\boldsymbol{m}]}{n!}\right)^{k_n} \tag{46}$$

where $k = \sum_j k_j$, with $j = 1,\dots,n$ and K is the set of all combinations of k_j such that $\sum_j jk_j = n$. For $n = 2$ there are only two such combinations, i.e. $\{k_1 = 0, k_2 = 1\}$ and $\{k_1 = 2, k_2 = 0\}$, corresponding to $k = 1$ and $k = 2$, respectively. The second derivative of $\mathcal{G}[\boldsymbol{q}[m]]$ is thus composed of two terms:

$$D^2\mathcal{G}[\boldsymbol{q}[m]] = (D^1\mathcal{G})_{\boldsymbol{q}[\boldsymbol{m}]}(D^2\boldsymbol{q}[\boldsymbol{m}]) + (D^2\mathcal{G})_{\boldsymbol{q}[\boldsymbol{m}]}(D^1\boldsymbol{q}[\boldsymbol{m}])^2 \tag{47}$$

Here $D^1\mathcal{G}$ and $D^2\mathcal{G}$ are the gradient and the Hessian of $\mathcal{G}$, respectively. Analogously, $D^1\boldsymbol{q}[\boldsymbol{m}]$ and $D^2\boldsymbol{q}[\boldsymbol{m}]$ are the Jacobian and the Hessian of $\boldsymbol{q}$, respectively. Elsewhere in the manuscript these differential operators are denoted as described in Sec. 1.2.

When expressing Eq. 47 explicitly in terms of the components of $\boldsymbol{q}$ and $\boldsymbol{m}$ we obtain Eq. 34.

References

[1] J. Fischbacher, A. Kovacs, M. Gusenbauer, H. Oezelt, L. Exl, S. Bance, and T. Schrefl, *Micromagnetics of rare-earth efficient permanent magnets*, J. Phys. D: Appl. Phys. **51**, 193002 1-17, (2018).

[2] J. Fujisaki, A. Furuya, Y. Uehara, K. Shimizu, T. Ataka, T. Tanaka, H. Oshima, T. Ohkubo, S. Hirosawa, and K. Hono, *Micromagnetic simulation of the orientation dependence of grain boundary properties on the coercivity of Nd-Fe-B sintered magnets*, AIP Advances **6**, 056028 1-9, (2016).

[3] D. Liu, T.Y. Zhao, R. Li, M. Zhang, R.X. Shang, J.F. Xiong, J. Zhang, J.R. Sun, and B. G. Shen, *Micromagnetic simulation of the influence of grain boundary on cerium substituted Nd-Fe-B magnets*, AIP Advances **7**, 056201 1-7, (2017).

[4] K. Schultz, and M. Schultz, *Micromagnetic study of equilibrium states in nano hemispheroidal shells*, J. Magn. Magn. Mater **442**, 332-337, (2017).

[5] H. Yuan, G. Wang, N.M. Dempsey, D. Givord, and D. Zeng, *Micromagnetic simulation of the effect of grain boundaries and secondary phases on the magnetic properties and recoil loops of hot-deformed NdFeB magnets*, J. Magn. Magn. Mater **491**, 165328 1-7, (2019).

[6] S.-K. Kim, *Micromagnetic computer simulations of spin waves in nanometre-scale patterned magnetic elements*, J. Phys. D: Appl. Phys. **43**, 264004 1-25, (2010).

[7] L. Exl, J. Fischbacher, A. Kovacs, H. Oezelt, M. Gusenbauer, and T. Schrefl, *Preconditioned nonlinear conjugate gradient method for micromagnetic energy minimization*, Comput. Phys. Commun. **235**, (17), 179-186, (2019).

[8] Q. Gong, M. Yi, and B.X. Xu, *Multiscale simulations toward calculating coercivity of Nd-Fe-B permanent magnets at high temperatures*, Phys. Rev. Materials **3**, (8), 084406 1-16, (2019).

[9] L. Exl, S. Bance, F. Reichel, T. Schrefl, H.P. Stimming, and N.J. Mauser, *LaBonte's method revisited: An effective steepest descent method for micromagnetic energy minimization*, J. Appl. Phys. **115**, (17), 17D118 1-3, (2014).

[10] C. J. García-Cervera, *Numerical Micromagnetics: a review*, Bol. Soc. Esp. Mat. Apl. **39**, 103-135, (2007).

[11] M. d'Aquino, *Nonlinear Magnetization Dynamics in Thin-films and Nanoparticles*, Doctorate Thesis, Università degli studi di Napoli "Federico II", 1-155, (2004).

[12] A. Hobza, C. J. García-Cervera, and P. Müllner, *Twin-enhanced magnetic torque*, J. Magn. Magn. Mater **458**, 183-192, (2018).

[13] C. Serpico, S. Perna, G. Bertotti, M. d'Aquino, A. Quercia, and D. Mayergoyz, *Noise-induced bifurcations in magnetization dynamics of uniaxial nanomagnets*, J. Appl. Phys. **117**, (17), 17A709 1-4, (2015).

[14] L. F. Shampine, and M. W. Reichelt, *The MATLAB ODE Suite*, SIAM J. Sci. Comput. **18**, 1-22, (1997).

[15] K.K. Nielsen, and R. Bjørk, *MagTense*, https://doi.org/10.11581/DTU:00000071 (2019).

[16] A. Smith, K.K. Nielsen, D.V. Christensen, C.R.H. Bahl, R. Bjørk, and J. Hattel, *The demagnetizing field of a nonuniform rectangular prism*, J. Appl. Phys. **107** (10), 103910 1-8, (2010).

[17] K.K. Nielsen, C.R.H. Bahl, A. Smith, and R. Bjørk, *Spatially resolved modelling of inhomogeneous materials with a first order magnetic phase transition*, J. Phys. D: Appl. Phys. **50** (41), 414002 1-9, (2017).

[18] S. Roman, *The Formula of Faà di Bruno*, Amer. Math. Monthly **87** (10), 805-809, (1980).

[19] K.K. Nielsen, A.R. Insinga, and R. Bjørk, *The Stray and Demagnetizing Field of a Homogeneously Magnetized Tetrahedron*, IEEE Magn. Lett. **10** 2110205 1-5, (2019).